

Binding affinity prediction of nanobody-protein complexes by scoring of molecular dynamics trajectories

Electronic Supporting Information

Miguel A. Soler^{*,1}, Sara Fortuna^{*,1,2}, Ario de Marco², Alessandro Laio¹

¹ SISSA, Via Bonomea 265, I-34136 Trieste, ITALY.

² Laboratory for Environmental and Life Sciences, University of Nova Gorica, Vipavska 13,
5000 Nova Gorica, Slovenia.

Corresponding authors:

* M.A.S.: miguelangel.solerbastida@sissa.it.

* S.F.: fortuna@sissa.it.

S1. Nanobody description and experimental methods.

The binding features of the anti-HER2 [1,2,3] VHHs used in this work have been described previously and are summarized in Table S1. In particular, the anti-HER2 nanobodies were isolated from a synthetic library [3] and characterized as described in [1]. They share the framework sequences and differ for their CDRs (Table S1), a condition which simplifies modelling and comparison. These VHHs were purified by metal ion affinity chromatography and successively by gel filtration for removing polymeric forms before measuring their affinity for HER2 [1]. Affinity constants were calculated by means of a Biacore T200 using a CM5 sensor chip (GE Healthcare) activated with 1000 resonance units of recombinant HER2 ectodomain [3]. VHHs at concentrations between 3.5 and 3000 nM were injected at 30 μ L/min for 120 sec with a regeneration time of 6 min (Figure S1). Affinity constants were calculated by means of the BT200 analysis software according to a 1:1 Langmuir binding model. Validation of the binding affinities was performed with a Proteon device (Biorad), as described in [1].

Overall, nanobodies with K_D values varying over a large range (0.08-900 nM) have been selected to assess the reliability of the *in silico* simulation under different conditions (Table S1).

Table S1 Experimental binding affinities, sequences of frameworks (F1-F4) and CDRs (CDR1-CDR3) of the EDHER2 VHH set considered in this work

EDHER2 set VHH code	K_D (nM)	F1	CDR1	F2	CDR2	F3	CDR3	F4
A10	4	F1	ATSNISN	F2	RAESRPL	F3	YMPLVRHKA	F4
G3	20		YTFSEET		WNHTFFE		VTPLPPNKA	
C8	34		DSYNESS		ARGNHPL		SMPMPKWKK	
D4	400		RYYEQSI		EYGGWQH		IRHQNQSM	
F7	700		YSSAAEV		WFHGETA		ENKPNEWGGQEM	
D9	900		GTSTTDG		SDASQEE		QYAFLDQEEPVIISW	
F1: VQLQASGGGFVQPGGSLRLSCAASG F2: MGWFRQAPGKEREFVSAIS F3: YYADSVKGRFTISRDNKNTVYLQMNSLRAEDTATYYCA F4: YWGQGTQVTVS								

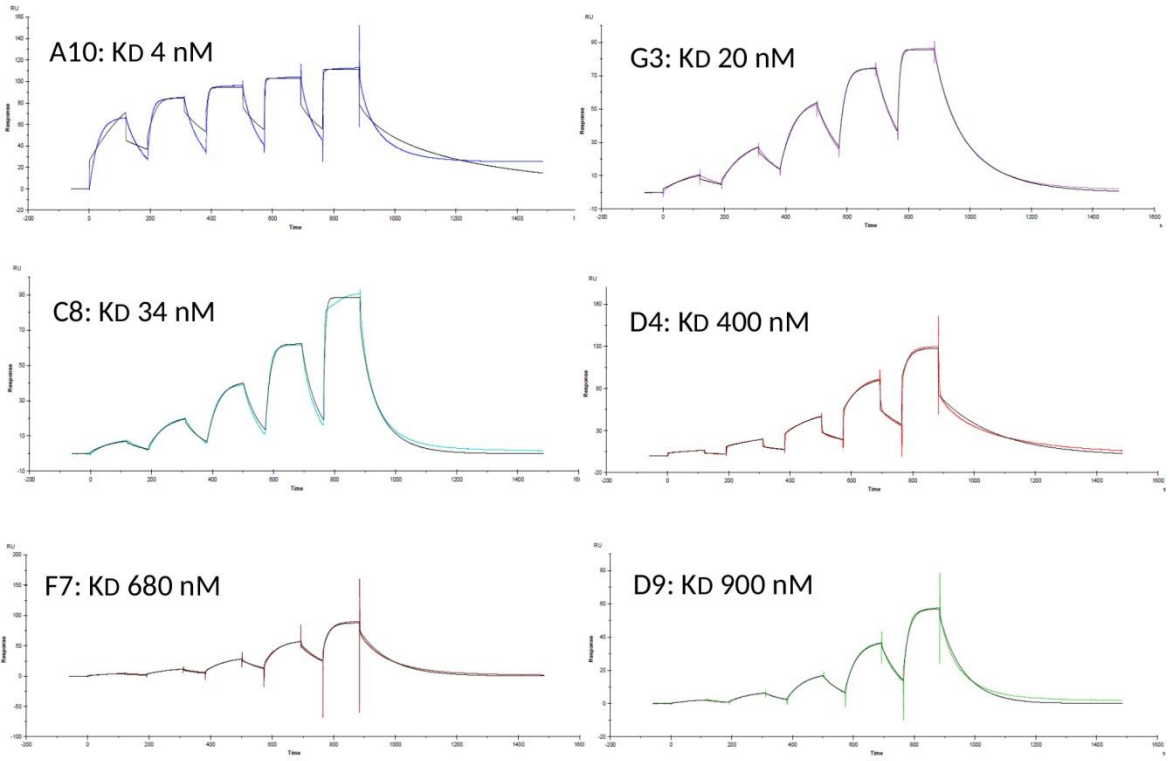


Figure S1. SPR sensograms of the 6 anti-HER2 VHHs.

S2. VHH Modelling

On each generated anti-HER2 VHH structure we run 200 ns MD simulations by using the same protocol detailed in the manuscript. We analyse the last 100ns of each simulation and for each VHH we choose for subsequent analysis the mutant with the lowest internal potential energy, namely those obtained from 3TPK for A10 and G3, while from 4POY for the others.

In Figure S2 we show the six mutants with the lowest internal potential energy. They present a structurally overlapping framework, while the variation of the loops gives rise to a variety of capturing surfaces. All the loops are unstructured with the exception of D4 which presents a short helix (Figure S3d).

The backbone root mean square deviation (RMSD, Figure S3a-f) shows the VHH models generated in this manner to be stable over time: their RMSD remains smaller than 0.1 nm. The root mean square fluctuation (RMSF, Figure S3g-l) is greater than 0.1 nm only in the CDR loops. Among the VHHs, only D4 seems to slightly diverge along the simulation with respect to both measures. Overall, their structure is stable over time. Only the variable part of the antibody is free to explore different conformations. The resulting VHHs have a variety of arrangements of their variable loops.

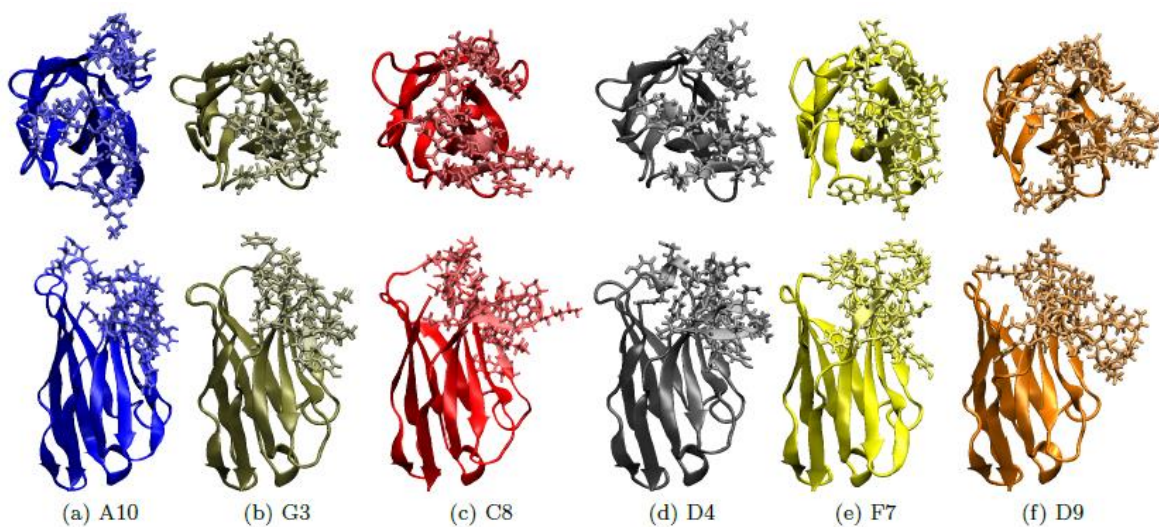


Figure S2 Top and side views of the lowest energy structures after 100ns MD run. The residues of the variable loops are shown.

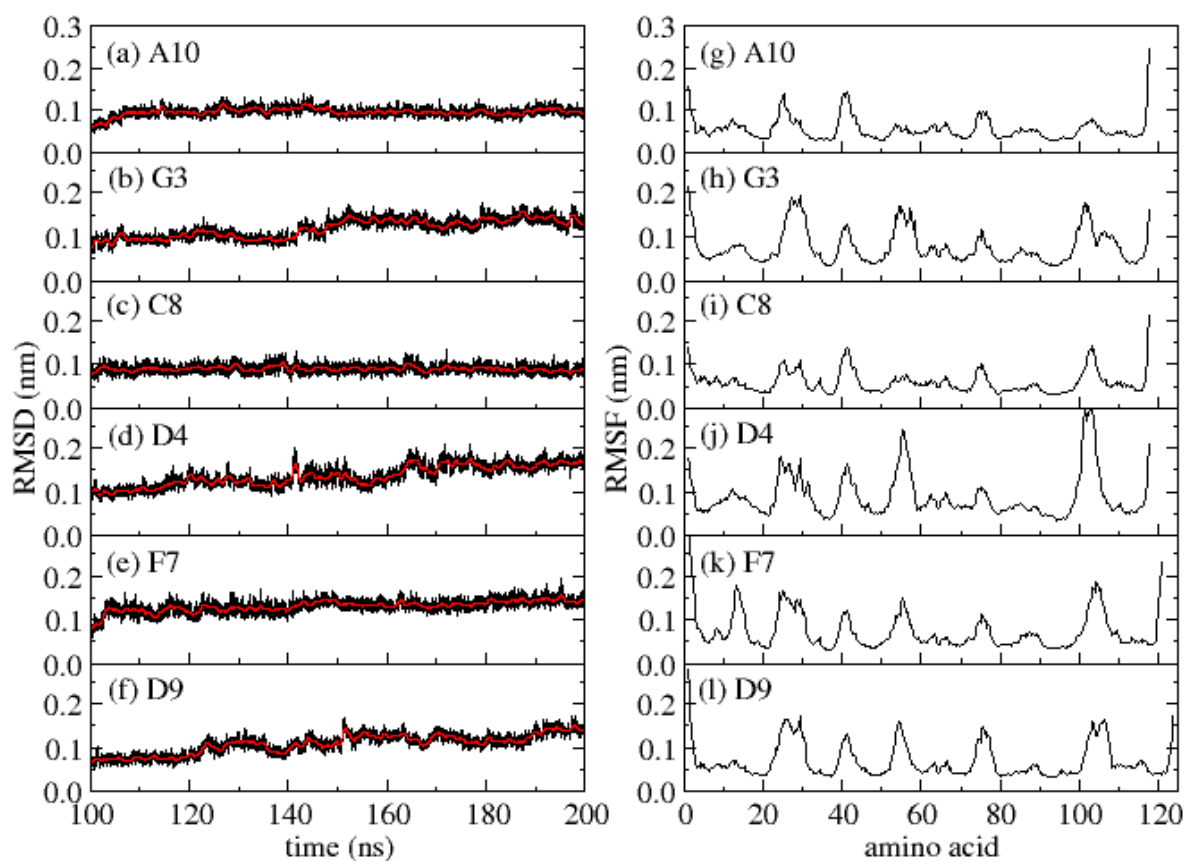


Figure S3 (a-f) Backbone RMSD (black solid line) with running averages over 1ns (red solid line), and (g-l) backbone RMSF calculated over the last 100 ns of MD simulation on the structures of Figure S2.

S3. VHH/EDHER2 Docking

The nanobodies have been experimentally shown to be displaced by Trastuzumab, therefore binding to the same site. We dock the VHH of Figure S3 to Trastuzumab EDHER2 binding site [4]. We performed the docking with the HADDOCK [5] webserver "easy interface" where system dependent active residues were defined for each VHH as their CDR, while for EDHER2 active residues were those in contact with Trastuzumab [6]: 579-583, 592-595, and 615-625. The comparison among representative structures of the HADDOCK most reliable complex cluster reveals different binding modes for each VHH-EDHER2 complex (Figure S4).

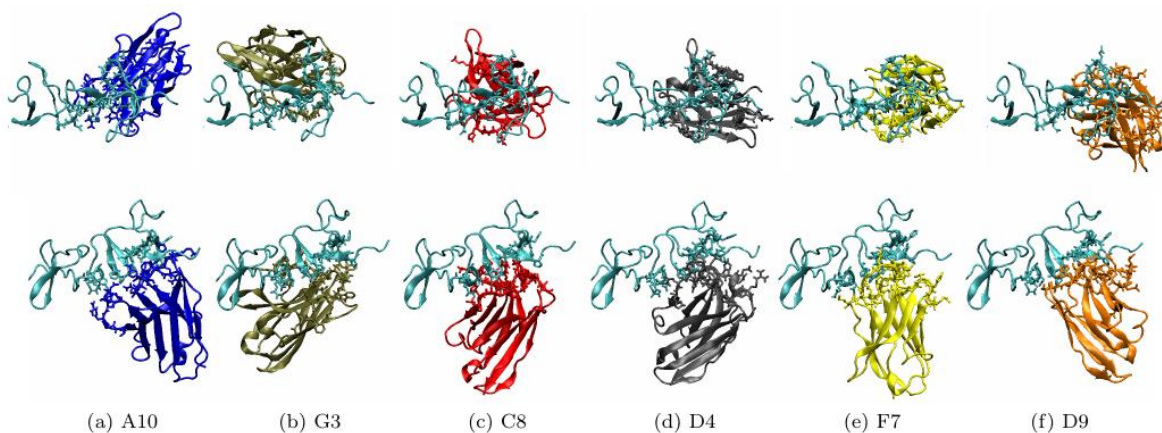


Figure S4 Top and side views of the HADDOCK complexes with the lowest scores. The amino acid side chains associated with the Trastuzumab binding site are highlighted on the EDHER2 domain (cyan), and those of the CDRs on the VHH.

S4. Binding score analysis

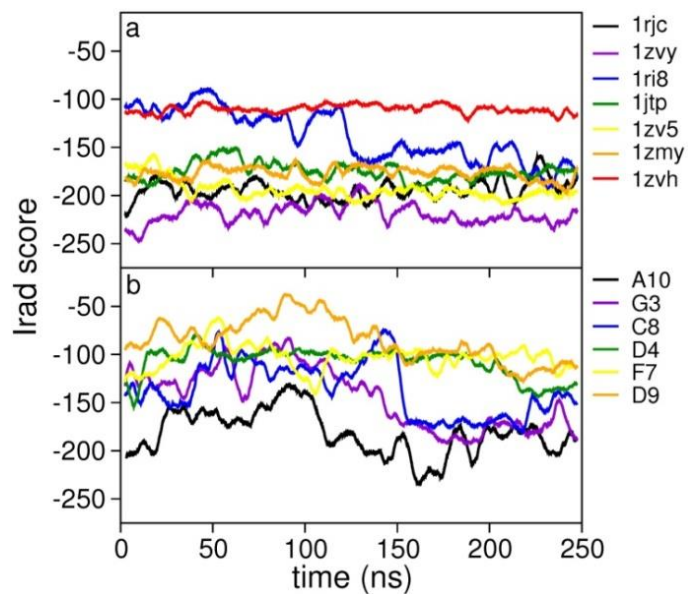


Figure S5 Evolution of the Irad binding score for (a) VHH-lysozyme and (b) VHH-EDHER2 complexes.

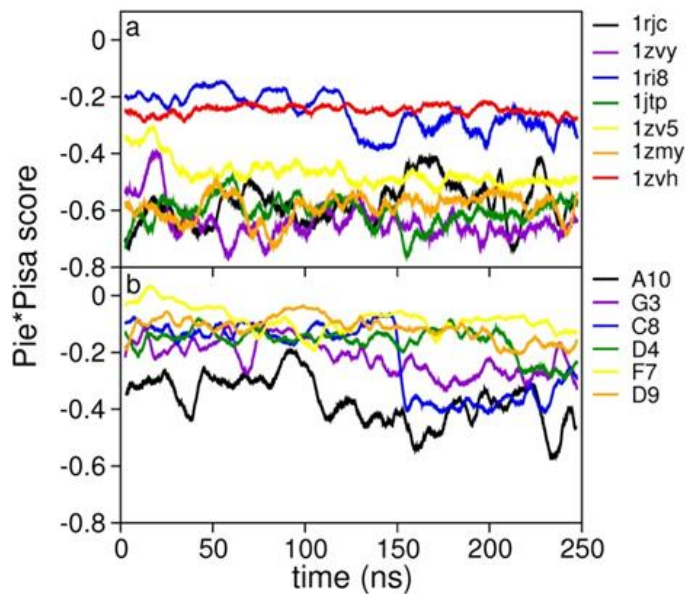


Figure S6 Evolution of the Pie*Pisa binding score (a) VHH-lysozyme and (b) VHH-EDHER2 complexes.

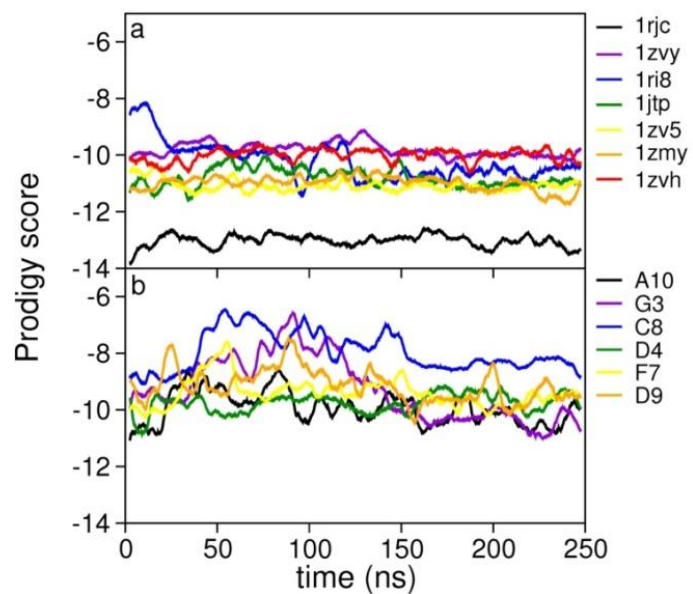


Figure S7 Evolution of the Prodigy binding score (a) VHH-lysozyme and (b) VHH-EDHER2 complexes.

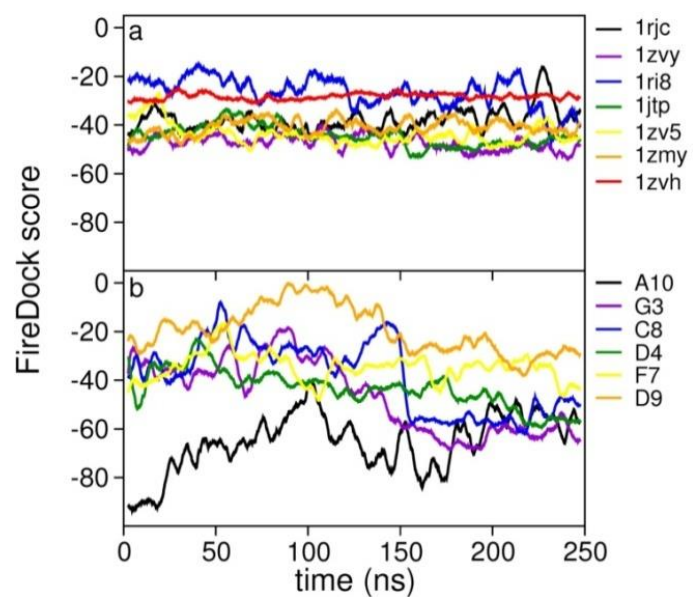


Figure S8 Evolution of the FireDock binding score (a) VHH-lysozyme and (b) VHH-EDHER2 complexes.

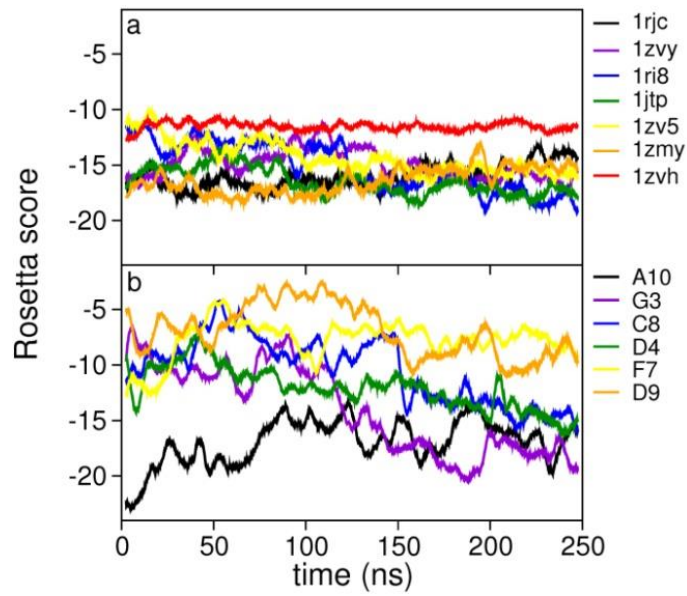


Figure S9 Evolution of the Rosetta binding score (a) VHH-lysozyme and (b) VHH-EDHER2 complexes.

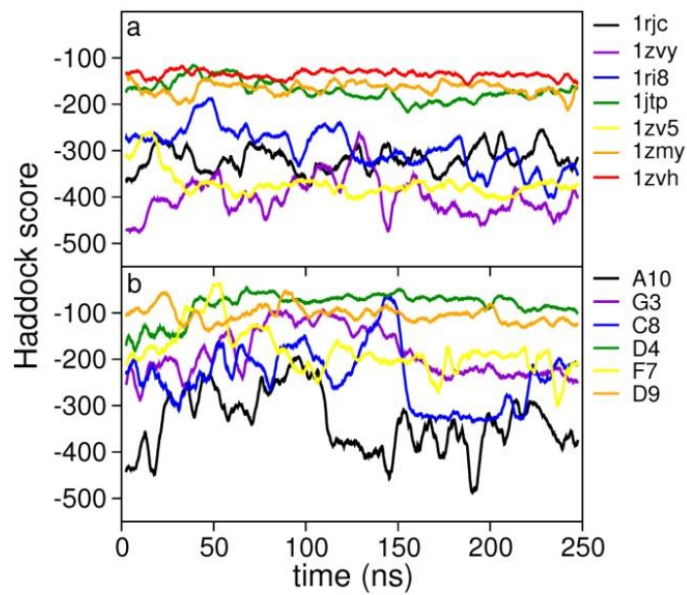


Figure S10 Evolution of the Haddock binding score (a) VHH-lysozyme and (b) VHH-EDHER2 complexes.

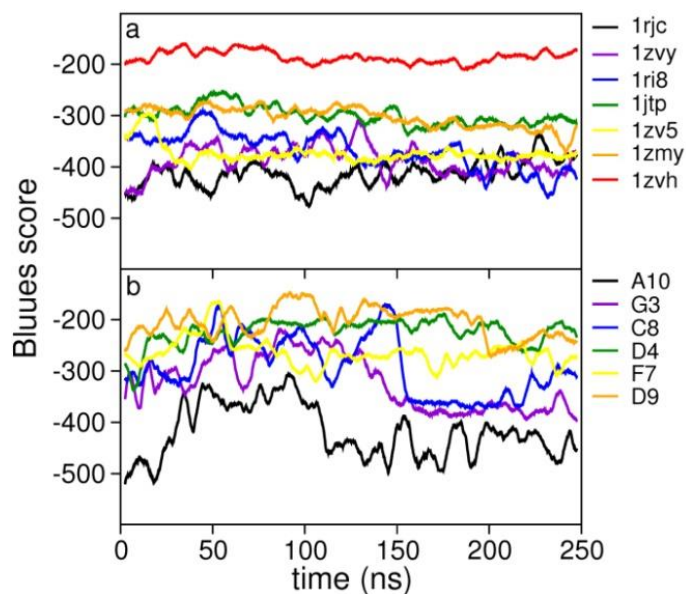


Figure S11 Evolution of the Blues binding score (a) VHH/lysozyme and (b) VHH/EDHER2 complexes.

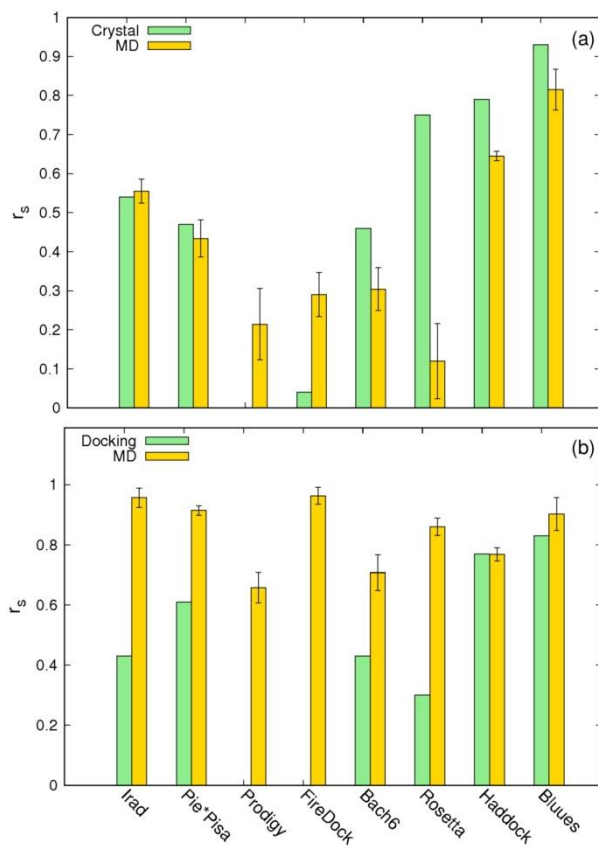


Figure S12. Spearman correlation between binding score average values and experimental binding affinities for the VHH-lysozyme (a) and VHH-EDHER2 (b) complexes. Only positive correlations are showed in the figure.

S7.REFERENCES

1 Djender, S.; Schneider, A.; Beugnet, A.; Crepin, R.; Desrumeaux K. E.; Romani, C.; Moutel, S.; Perez, F.; De Marco, A. Bacterial Cytoplasm as an Effective Cell Compartment for Producing Functional VHH-Based Affinity Reagents and *Camelidae* Igg-Like Recombinant Antibodies. *Microb. Cell Fact.* **2014**, 13, 140.

2 de Marco, A. *Isolation of Recombinant Antibodies that Recognize Native and Accessible Membrane Biomarkers*. In: T.A. Camesano (ed.), *Nanotechnology to Aid Chemical and Biological Defense*, NATO Science for Peace and Security Series A: Chemistry and Biology, pp. 49-66, Springer: Dordrecht, The Netherlands, 2015.

3 Moutel, S.; Bery, N.; Bernard, V.; Keller, L.; Lemesre, E.; De Marco, A.; Ligat, L.; Rain, G. C.; Favre, G.; Olichon, A.; Perez, F. Nali-H1: A Universal Synthetic Library of Humanized Nanobodies Providing Highly Functional Antibodies and Intrabodies. *eLife* **2016**, 5, e16228.

4 Cho, H.S.; Mason, K.; Ramyar, K. X.; Stanley, A. M.; Gabelli, S. B.; Denney Jr., D. W.; Leahy, D. J. Structure of the Extracellular Region of HER2 Alone and in Complex With the Herceptin Fab. *Nature* **2003**, 421, 756-760.

5 van Zundert, G. C.; Rodrigues, J. P.; Trellet, M.; Schmitz, C.; Kastiris, P. L.; Karaca, E.; Melquiond, A. S.; van Dijk M.; de Vries S. J.; Bonvin A. M. The HADDOCK2.2 Web Server: User-Friendly Integrative Modeling of Biomolecular Complexes. *J. Mol. Biol.* **2016**, 428, 720-725.

6 H. S. Cho, K. Mason, K. X. Ramyar, A. M. Stanley, S. B. Gabelli, D. W. Denney Jr. and D. J. Leahy, *Nature*, **2003**, 421, 756-760.